On the design of a small scale tidal converter for long time deployment at sea

D. Alizzio, L. Gurnari, V. A. Nardi, M. Torresi, D. Coiro, S. Camporeale, P. Filianoti

Abstract—**This paper presents the design of a scale model of a kite-like tidal converter, GEMSTAR, intended for long-term deployment at sea. The main objective of this experiment is to develop a digital twin with integrated fault detection and isolation capabilities to improve the reliability and performance of the system. A fully functional 1:10 scale model of GEMSTAR was designed based on extensive measurements of tidal currents at the planned deployment site. Several locations were investigated to determine the most suitable flow profiles for energy generation. This study outlines the key challenges for operational functionality and describes the selection of critical physical parameters to be monitored during deployment using onboard sensors.**

Index Terms—**Tidal currents; energy converters; operative matching; 3D-scanning; hydrokinetic turbine; BEMT theory.**

I. Introduction

According to the Paris Agreement, at least 60% of the world's electricity must be generated from renewable sources by 2030. To achieve this target, the expansion of renewable energies must be significantly accelerated, with the average annual growth rate of 6% observed between 2019 and 2021 doubling by 2030 [1]. However, mature technologies such as hydropower can only make a limited contribution to this growth, so there is a need to explore less conventional renewable sources. Marine energy, which includes wave and tidal resources, offers significant potential for renewable energy generation. Wave energy technologies harness the kinetic and potential energy of ocean waves using devices such as point absorbers [2], [3], oscillating water columns [4], [5], and overtopping devices [6], [7]. These systems face challenges in terms of efficiency [8], durability [9], and grid integration [10]. Tidal energy uses the predictable currents of the tides with the help of tidal turbines and tidal barrages. Tidal systems are more predictable and reliable, but require high installation costs and special site conditions. Both technologies (wave and tidal) have significant potential for renewable energy generation, but require further advances in design, cost reduction and environmental impact assessment to be commercially deployed on a large scale. The idea of harnessing tidal energy dates back to the Roman era, when tidal mills were used along riverbanks to harness the rise and fall of the tides. Tidal energy remains an attractive renewable resource due to its predictability, which is determined by astronomical forces, and its smaller environmental footprint compared to other renewable technologies [11]. Several studies have assessed the potential of tidal energy. Black and Veatch Consulting Ltd. estimates a range of practical energy generation of 10-30 TWh / year for the UK alone [12], [13].

A variety of tidal energy conversion technologies are moving towards commercialization and a large body of scientific literature addresses key issues related to tidal stream energy generation. These technologies harness the energy of ocean currents, river currents and tidal-induced water movements. The main technological solutions can be divided into three [14]: hydrokinetic turbines on floating platforms (either underwater or on the surface), bottom-mounted hydrokinetic turbines (similar to offshore wind farms) and subsea kite-like devices equipped with hydrokinetic turbines.

Several research projects are looking at different technological aspects of tidal energy generation. For example, a comparative study in [15] assesses the efficiency and carbon footprint of a wave energy device (Oyster) and a bottom-mounted tidal turbine (SeaGen). In addition, [16] presents a comprehensive economic analysis of tidal power technologies, highlighting the economic feasibility of floating plants. In [17] an experimental study of a moored tidal power plant was conducted, although the system was only operated on battery power for a limited time. Furthermore, [18] investigates efficiency issues , using real data to improve the Blade Element Momentum (BEM) model.

Recent research trends also emphasize the integration of tidal energy systems into broader coastal and estuarine management plans and promote multidisciplinary research efforts [19]. For further insights into several comprehensive reviews of tidal energy tech-

Part of a special issue for EWTEC 2023. Original version published in EWTEC 2023 proceedings at https://doi.org/10.36688/ewtec-2023-567.

Manuscript submitted 10 January 2025; Accepted 2 May 2025. Published 31 May 2025.

This article has been subject to single-blind peer review by a minimum of two reviewers.

This work was supported by the Italian Ministry of University and Research under the project PRIN "SMART (Sea wave energy converters and MARine Tidal turbines) - PIANO NAZIONALE DI RIPRESA E RESILIENZA (PNRR) Missione 4 "Istruzione e Ricerca" - Componente C2 Investimento 1.1, "Fondo per il Programma Nazionale di Ricerca e Progetti di Rilevante Interesse Nazionale (PRIN)", 2022.'

D. A., L. G., V. A. N., and P. F. authors are with University Mediterranea of Reggio Calabria, Via dell'Università, 25, 89124 - Reggio Calabria, Italy email:{damiano.alizzio, luana.gurnari, vito.nardi, filianoti}@unirc.it

D. C. author is with University of Naples Federico II, Via Claudio 21, 80125 - Napoli, Italy email: domenico.coiro@unina.it.

M. T. and S. C. authors are with Polytechnic of Bari, via Amendola 126/b, 70126 - Bari, Italy email:{marco.torresi, camporeale}@poliba.it

Digital Object Identifier:
https://doi.org/10.36688/imej.8.237-246

nologies, see [14], [19], [20], [21].

The GEMSTAR tidal converter belongs to the category of underwater kite-like devices. It is a submerged, floating system (see Figure 1) that is attached to the seabed with a flexible mooring cable. The system harnesses the energy of tidal currents via two symmetrical hydrokinetic turbines, each equipped with three composite blades. The GEMSTAR turbine is able to adapt to changing current directions by rotating freely [11]. The system was developed by SEAPOWER, a non-profit consortium for applied research associated with the University of Naples Federico II [20], [21].

The GEMSTAR solution offers several advantages, including reduced maintenance costs due to easy handling out of the water, the absence of active rotating control components and the self-aligning properties. A performance comparison conducted in [22] through real-world simulations has shown that GEMSTAR achieves almost twice the efficiency of its closest competitor among existing technologies. A new scaled-down model of GEMSTAR is currently being deployed in the Strait of Messina near the Marine Energy Lab (RENEW-MEL) [23].

The Strait of Messina is an ideal location for tidal energy generation due to the size and regularity of the current velocities, making it one of the most promising sites in the Mediterranean [24], [25]. The recorded maximum current velocities in the Strait are between 1.8 m/s and over 3 m/s and follow a semi-diurnal pattern [26], [27]. The annual energy generation potential of the tidal currents in the Strait is estimated at up to 125 GWh/year, taking into account the accessible depths [22].

The deployment of GEMSTAR includes the long-term operation of the device and focuses on addressing critical challenges such as active attitude control to prevent cable twisting and optimize alignment with tidal currents. In addition, fault detection and isolation (FDI) and predictive maintenance techniques are implemented to improve the reliability [28].

Another critical issue we have to deal with during extended deployments is marine biofouling, which poses a threat to the efficiency of the tidal turbines and the stability of the power supply. Despite its importance, the impact of biofouling on tidal power plants is still poorly understood. Research focuses on the effects of surface roughness caused by biofouling on hydrokinetic turbines.

The aim of this paper is to provide a detailed overview of the design considerations and operational strategies for small-scale GEMSTAR deployment. The paper is organized as follows: Section II provides a detailed characterization of the ocean currents at the deployment site. Section III outlines the geometry and operating parameters of the system. Section IV discusses the kinetic energy conversion analysis, while Section V discusses the power conversion strategies. Finally, Section VI provides an overview of the measurement architecture for data acquisition and monitoring.

Fig. 1. A render of the GEMSTAR model to be installed off the beach of Reggio Calabria.

Fig. 2. A map of the RENEW-MEL site in the Strait of Messina. The placeholder indicates the position of the laboratory.

II. Characterization of the Deployment Site

Each potential site for the use of tidal energy has unique characteristics that need to be thoroughly analysed, in order to assess its energy production potential. Several studies, including those conducted by the Italian Hydrographic Institute [29], [25], have examined the tidal currents in the Strait of Messina. Despite significant variations in current speed, a semi-diurnal pattern caused by the tides can be observed, with four daily peaks in speed.

The proposed installation site is located in the city of Reggio Calabria (see Figure 2), along the Calabrian coast of the Strait of Messina. The coastline runs SW-NE and the Marine Energy Lab (RENEW-MEL) is located near the mouth of the Calopinace river (see

Figure 3). At this location, the tidal currents show significant spatial variations due to the proximity to the coast, the topography of the seabed and the local coastal orientation.

In order to take this variability into account, measurements of the flow velocity were carried out at three different locations over the course of a one-year monitoring campaign. These positions, labeled A, B and C, are shown in Figure 3:

- Position A: this location is closest to the mouth of the Calopinace River and was monitored from December 2020 to March 2021 using a Nortek AWAC AST 600 kHz Acoustic Wave and Current Profiler. The device was installed at a depth of 7 meters below sea level to determine the influence of the river mouth on current speed and direction.
- Position B: this is the deepest location studied. It was selected to assess the variability of current speed and direction along the water column in an area less affected by coastal influences. The measurements were carried out with the same Nortek AWAC AST 600 kHz profiler from April to November 2021, with the device installed 16 meters below sea level.
- Position C: the closest location to the coast, which is in a sheltered area due to a coastal headland. This position was monitored from October to November 2020, using the Nortek AWAC AST 600 kHz profiler, with the device installed at a depth of 6 meters.

To assess the spatial variability of the tidal currents, polar diagrams of the current speed classes were created for the three locations (see Figure 4). Even if the current directions can be compared across all locations, the frequency of the individual speed classes can vary due to the non-simultaneous measurement periods at the different locations.

As can be seen in Figure 4, the most frequent current speed was recorded at location A at a depth of 2 meters below sea level and was between 0.5 and 0.75 m/s (represented by the green line), with a south-southwest (SSW) direction. This speed occurred 18 % of the time, which corresponds to approximately 65 days per year. The second and third most frequent speed classes were 0.75 to 1 m/s and 1 to 1.25 m/s, also in a SSW direction, and occurred approximately 22 days and 15 days per year, respectively.

At position B, the current speed was between 0.5 and 0.75 m/s, measured at a depth of 4 m below sea level, and occurred on 20 days per year. The prevailing ebb current (i.e. the current flowing towards the Ionian Sea or south) dominates both at position A and position B. The ebb current at position B flows almost parallel to the coastline, while at position A it flows at an angle of about 40°.

At position C, which is closest to the coast, there are currents that run almost perpendicular to the coastline, similar to currents induced by wave breaking. Due to its sheltered location, this site is less affected by large tidal currents.

Figure 5 shows the typical current speed profile along the z-axis for the three sites. The maximum current velocity was observed at positions A and C at a depth of 2 meters below the sea surface, while at position B the highest velocity was measured at the water surface.

The installation depth for the GEMSTAR device was set at 2 meters below the water surface, as shown in Figure 4. This depth was chosen to ensure safe navigation while remaining shallow enough to detect higher current velocities.

The absence of a flood current (*i.e.* a current flowing towards the Tyrrhenian Sea or to the north), as seen in Figure 5, is also confirmed by Figure 6, which shows a four-day time history of the current speed at position A (blue line). Instead, a constant ebb current velocity of around 0.6 m/s was recorded during the times when the flood current would be expected. These secondary currents, which move in the opposite direction to the main current, are commonly referred to as "bastard currents" and are often observed near the coast.

Based on the above analysis, position A appears to be the most suitable location for the GEMSTAR device as it is closest to the river mouth and has a design speed of 0.9 m/s, which corresponds to the average current speed during the observation period.

A harmonic analysis of the current speed records at the three sites was performed using the T-Tide tool in the MATLAB environment [26], [27]. This tool is often used for the harmonic analysis of tidal data and enables a comparison with values from the literature [22]. By filtering out the constant components from the recorded data, the spectral composition of the gravitational tidal constituents was determined. Table I shows the 20 most important components in order of amplitude. These components were used to calculate a prediction of the current velocity. The orange line in Figure 6 shows the predicted current speed, which underestimates the actual speed by about 13%.

Fig. 3. Three hypothetical installation sites of the current energy converter, where the measurement campaign was conducted.

III. The turbine rotor geometry and working parameters

A vertical view of the positioning of the GEMSTAR device during operation is shown in Figure 7. The

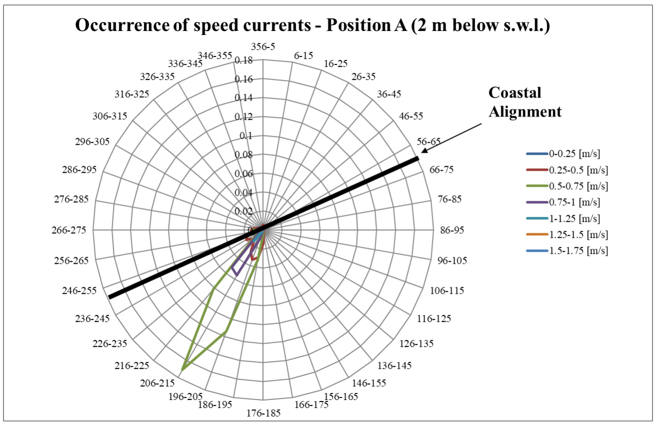

(a)

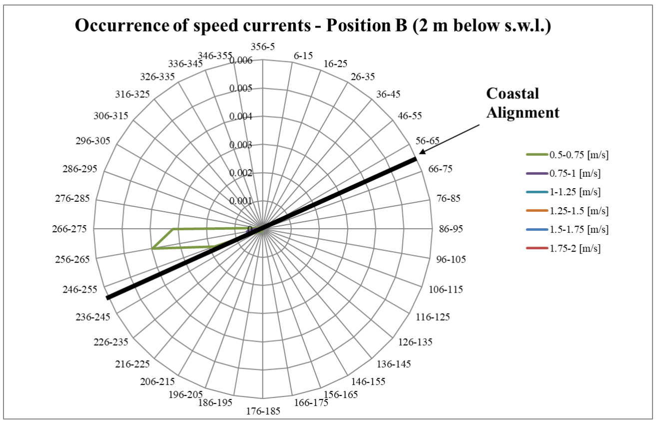

(b)

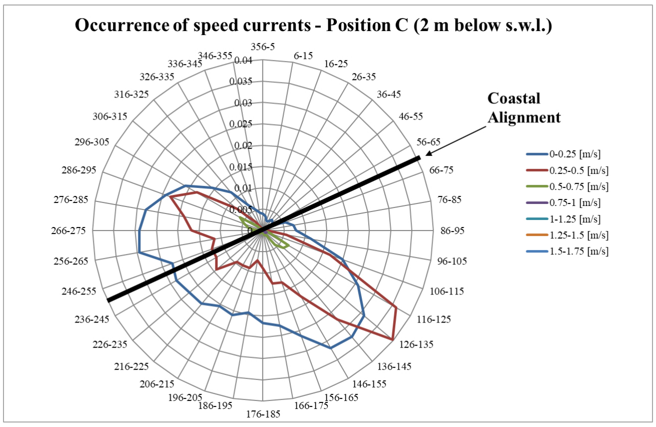

(c)

Fig. 4. Frequency of speed and direction of currents occurring in the three locations indicated in Figure 3.

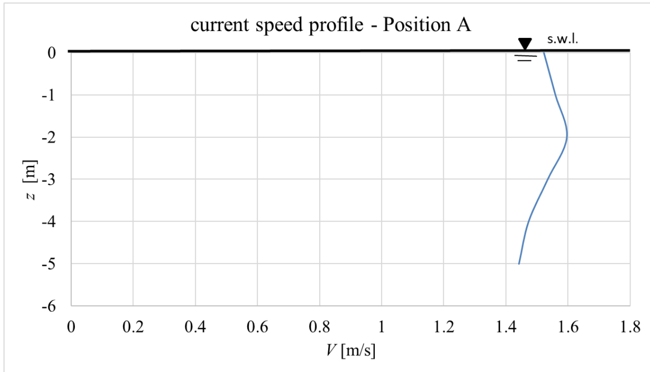

(a)

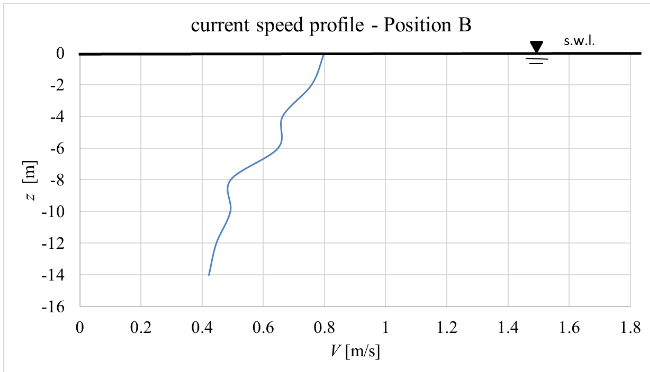

(b)

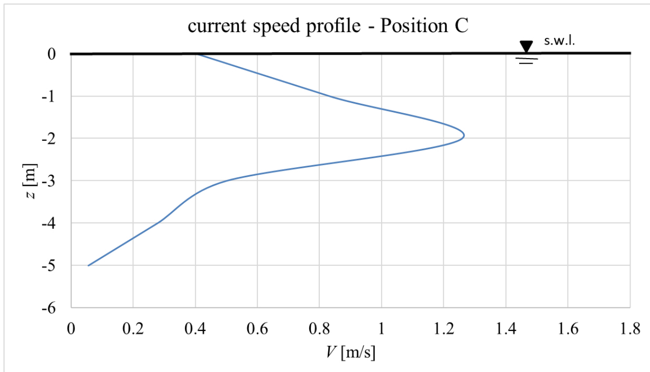

(c)

Fig. 5. Current speed profile in the three locations indicated in Figure 3.

optimal vertical position of the device z, is where the highest values of current velocity occur, along the vertical axis of the installation site. Furthermore, the vertical position of the device effectively depends on the mixture of buoyancy and drag forces. The more the flow velocity increases, the deeper the device dives. As can be seen in the Figure 7, the minimum specification z_{min}, represents the rest position of the system (*i.e.* in the absence of current). The value of z_{min}, can be assumed to be equal to the sum of half the height of the maximum expected wave, the absolute maximum amplitude of the tide and a safety distance (*i.e.*, one and a half rotor radii R). Thus, the working depth of the device $d_0 - d_{min}$, depends on the angle of inclination β, through the following condition:

$$\beta = \arcsin\left(1 - \frac{d_0 - d_{min}}{d_0}\right). \tag{1}$$

The angle β_{min}, depends on the tension applied to the mooring line:

$$\beta_{min} = \arctan\left(\frac{F_V}{F_{0,max}}\right), \tag{2}$$

where F_V, is the buoyancy force and $F_{0,max}$, is the sum of the thrusts exerted by the two rotors during the flow at maximum speed. Table II summarizes the geometric configuration of the system subjected to V_{max} = 1.6 m/s. To obtain this working configuration, we must calculate $F_{0,max}(V_{max})$ and fix the value of F_V, in order to obtain the indicated β_{min}.

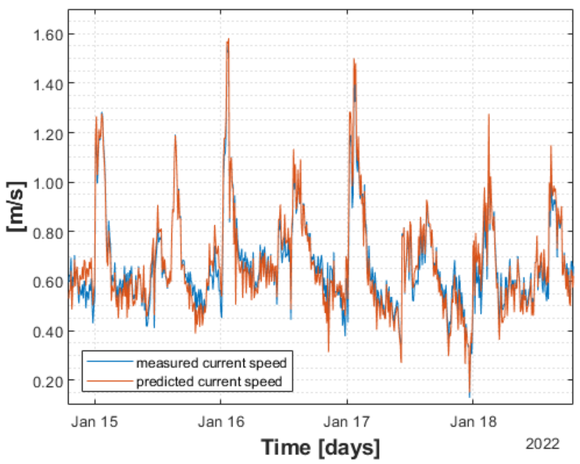

Fig. 6. Time history of the current speeds at location A of the Figure 3: comparison between predicted and measured current speed.

TABLE I
SUMMARY OF HARMONIC ANALYSIS RESULTS: POSITION A

Constituent name	Freq. cph	Period h	Amplitude m/s	Phase °
'*MM'	0.0015	661.2882	0.0794	60.66
'*M2'	0.0805	12.4206	0.0544	37.21
'*MSF'	0.0028	354.3712	0.0385	76.45
'*K1'	0.0418	23.9345	0.0263	310.05
'*MN4'	0.1595	6.2692	0.0242	209.85
'*MK3'	0.1223	8.1771	0.0201	38.05
'*NO1'	0.0403	24.8332	0.0195	221.78
'*S2'	0.0833	12.0000	0.0171	74.88
'*M4'	0.1610	6.2103	0.0161	181.28
'*MO3'	0.1192	8.3863	0.0158	136.64
'*MS4'	0.1638	6.1033	0.0145	256.27
'*MU2'	0.0777	12.8718	0.0137	260.66
'*UPS1'	0.0463	21.5782	0.0121	164.67
'*N2'	0.0790	12.6584	0.0118	338.62
'*2Q1'	0.0357	28.0062	0.0117	28.97
'*Q1'	0.0372	26.8684	0.0113	160.43
'*L2'	0.0820	12.1916	0.0108	108.83
'*ETA2'	0.0851	11.7545	0.0098	90.51
'*SN4'	0.1623	6.1602	0.0097	226.94
'*M3'	0.1208	8.2804	0.0090	218.49

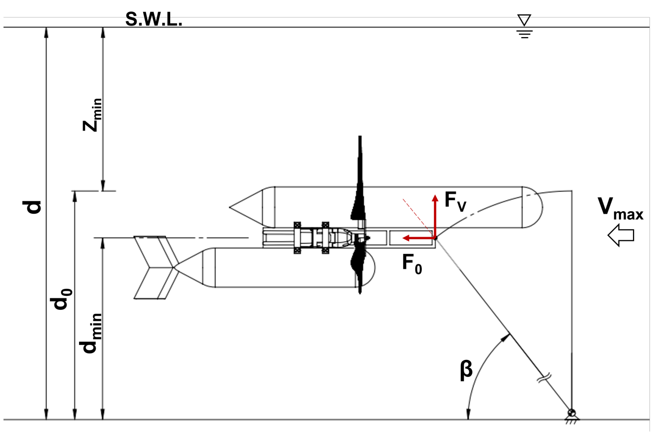

Fig. 7. A vertical view of the GEMSTAR device during operational.

Using the Blade Element Momentum Theory (BEMT), the performance of the rotor was investigated and the characteristic curves were generated. Under the effect of the typical flow velocities occurring at the installation site, the theoretical performance and the thrust of the rotor during the period of use were evaluated. These results represent the input parameters for the design of the energy converter. Taking into account the speed distribution at the installation site, a rotor diameter of 1.2 m was selected to ensure rotation of the blades at low speeds. The actual blade geometry was precisely verified by laser scanning. For this purpose, an Artec EVA 3D scanner was used, which has an accuracy of ±0.1 mm. The blade model was then sliced along its radial axis, and 23 sections of the airfoil were extracted. The leading and trailing edges were recognised for each section and thus measurements of the chord length c and the angle of attack α, were taken. A further comparison with the physical model of the blade resulted in a maximum error of ±0.09 mm in the chord length. Figure 8 shows the physical blade (a) and the mesh for the corresponding 3D reconstruction (b). The blades will be recovered and scanned at regular intervals to assess the impact of bio-fouling. Computational fluid dynamics (CFD) simulations are then performed on the scanned real surface and the new performance is compared to the previous one to track and quantify the impact of bio-fouling on the performance of the rotor.

TABLE II
GEOMETRIC CONFIGURATION OF GEMSTAR DEPLOYMENT.

d [m]	7
z_{min} [m]	2
$d_0 - d_{min}$ [m]	0.5
β_{min} [deg]	65

IV. THE KINETIC ENERGY CAPTURED BY THE ROTOR

After scanning the rotor blade and normalizing the mesh slices with respect to their own chord length, the drag and lift coefficients were estimated using the open-source code X-Foil by combining a vortex panel method for inviscid flow, boundary layer equations for viscous effects, transition and separation predictions, and an iterative viscous-inviscid coupling for accurate convergence. Applying the Blade Element Momentum Theory to the rotor reconstructed from the detected sections, the characteristic curves of the turbine were generated. The hydrodynamic thrusts of the rotors were calculated with respect to the rotational speed of the rotor itself and parameterized with respect to the speed of the fluid current. In the same way, the theoretical mechanical power intercepted by the rotor was calculated as a function of the rotational speed n and parameterized with the current velocity. These curves also make it possible to estimate the curves of the maximum torque and the maximum power that can be captured as a function of the current velocity V. The Figures 9 and 10 show the theoretical torque and mechanical power available on the machine axis, respectively. The family of curves is drawn for different values of current velocity from 0.5 m/s to 1.75 m/s in an interval of 0.25 m/s. The black dashed line connects the maximum of each curve. Similarly, Figure 10 shows the power at the hub of the rotor as a function of the rotational speed n. The black dashed line has the same meaning as in Figure 9. In the plane (n, V) it can be easily represented by a linear relationship:

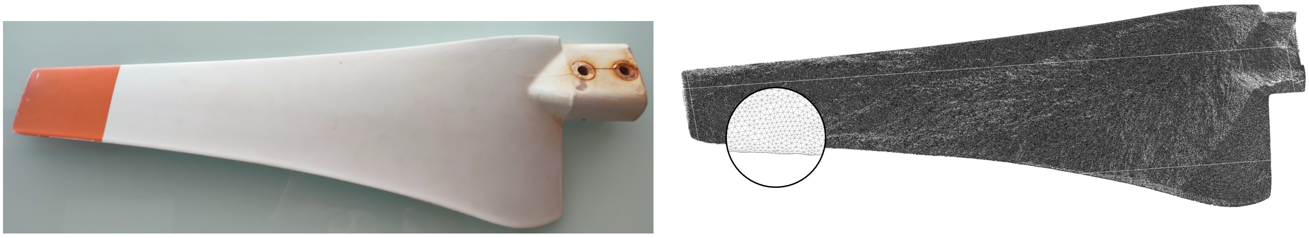

(a) (b)

Fig. 8. GEMSTAR a) rotor blade and b) mesh captured by the 3D-scanner.

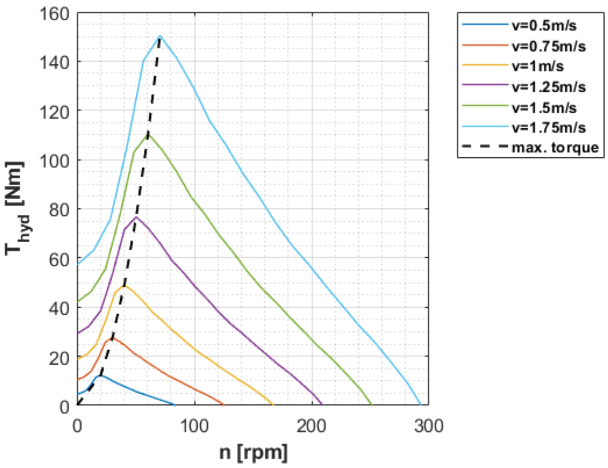

Fig. 9. Theoretical torque of the turbine rotor as a function of the rotational speed n, for several values of the current speed.

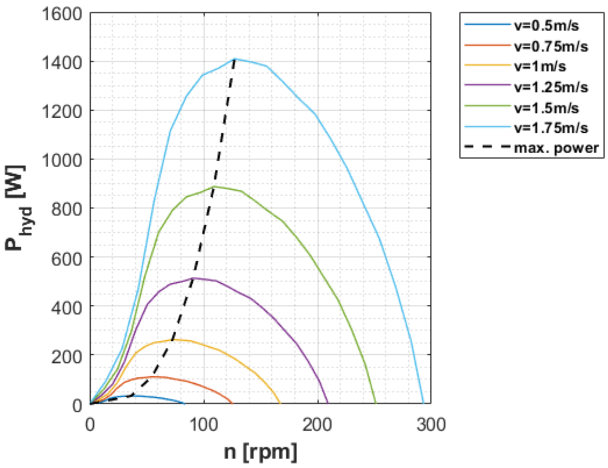

Fig. 10. Theoretical mechanical power of the turbine rotor.

$$n = 72.7V, \tag{3}$$

where n is the angular speed of the turbine rotor in [rpm] and V is the water speed in [m/s]. This relationship is useful for implementing control strategies aimed at maximizing power generation. The torque T_0 exerted by a current with a given velocity V when the rotor is stopped is shown in Figure 11 and can be

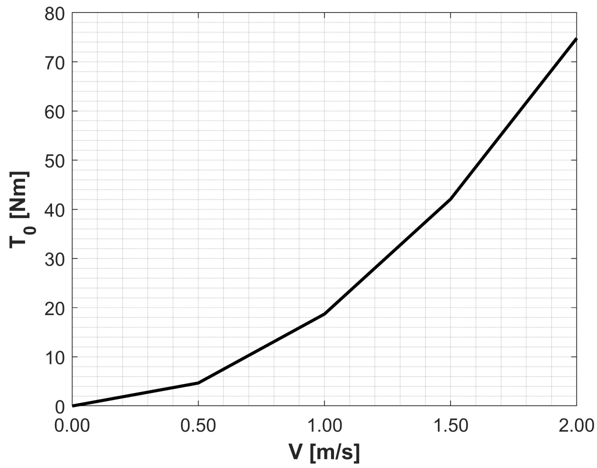

Fig. 11. Rotor starting torque as function of the current speed V.

interpolated by the quadratic relation:

$$T_0 = 18.7V^2, \tag{4}$$

It is useful to determine the minimum speed of the current at which the rotation can be started.

Taking into account the maximum power of each rotor, which is shown in Figure 10, two electric generators with a rated power of 1.4 kW are selected. The maximum thrust $F_{0,max}$ exerted by a current with $V_{max} = 1.6$ m/s is 1014 N. Considering Eq. 2, F_V must be equal to 2940 N in order to maintain the angle of inclination β of the mooring line at the desired value of 65°. The mechanical power absorbed by the flow is then transmitted to two Brushless Direct Current (BLDC) electric generators mounted downstream the rotor shafts. Brushless direct current (BLDC) machines with permanent magnets are a popular choice for renewable energy generation as they offer several advantages in terms of durability, a wide operating range, high efficiency, low maintenance and power density [28]. This is mainly due to the absence of moving contact elements (brushes), whose abrasion is the main cause of fault in conventional DC generators, followed by commutation sparks [30]. The experimental apparatus described in this paper uses two Nanotec DC80 BLDC motors as power generators. Therefore, no data is available to characterise the DC80 as a generator. A suitable characterization procedure must be applied to determine the required mechanical power as a function of angular speed and the electrical power as a function of angular speed when the electrical load is varied. On the other hand, axis torque versus electrical load measurements bring up information about the cogging torque of the DB80 as a generator. An ad hoc test rig was developed. It includes a DC motor that supplies the generator with a known mechanical power via a rigid joint and an electrical load for the dissipation of the generated electrical power. The test rig is equipped with sensors that measure the speed of the drive motor/generator system and the current and voltage applied to the load. During characterization procedure, the system is driven at various velocity setpoints using closed loop control to achieve stable velocity and smooth transient response.

V. The Mechanical Efficiency of the System

The quota of the tidal current that can be captured has been evaluated through the BEM. Several control strategies can be used to maximize current generation. An attractive choice is velocity control: power is generated at constant rotational speed by reducing the absorbed torque and increasing the speed of the generator [31]. With this approach, the rotor operates in a flux-wakening condition [11]. The torque is driven by a speed multiplier of 1:20 to meet the electrical characteristics of the generator. An estimate of the power loss in the steady state during the drive was made by taking into account the loss contribution of each drive parts. The following efficiency coefficients were defined for P_{TOT}, the reference tidal power, which refers to the undisturbed water velocity V and flows through the area S swept by the rotors, P_{hyd} the hydraulic power available at the rotor hub, P_m the mechanical power available at the generator shaft and P_{el} the achievable electrical power:

$$P_{EL} \equiv \eta_{el}\eta_m c_{P,hyd} P_{TOT} \equiv c_P P_{TOT}, \tag{5}$$

where $\eta_{el} \equiv \frac{P_{EL}}{P_M}$, is the electrical efficiency of the generator, $\eta_m \equiv \frac{P_M}{P_{HYD}}$, is the mechanical efficiency of power drive and $c_{P,hyd} \equiv \frac{P_{HYD}}{P_{TOT}}$, is the hydraulic power coefficient of the rotors. Overall,

$$c_p \equiv \eta_{el}\eta_m c_{P,hyd}, \tag{6}$$

is the power coefficient of the entire conversion chain. The power coefficient c_p together with its factors depends on rotational speed. The hydraulic power coefficient can be expressed as follows

$$c_{P,hyd} \equiv \frac{P_{HYD}}{0.5\rho S V^3} \tag{7}$$

as the ratio between the hydraulic power intercepted by the rotor and the reference power of the tidal current $P_{TOT} = 0.5\rho S V^3$. In general, $c_{P,hyd}$ is expressed as a function of the Tip Speed Ratio TSR:

$$TSR \equiv \frac{\omega R}{V}, \tag{8}$$

where ω is the angular velocity of the rotor. Figure 12 shows the expected values of the $c_{P,hyd}$ coefficient for one of the two rotors of the GEMSTAR device as a function of TSR.

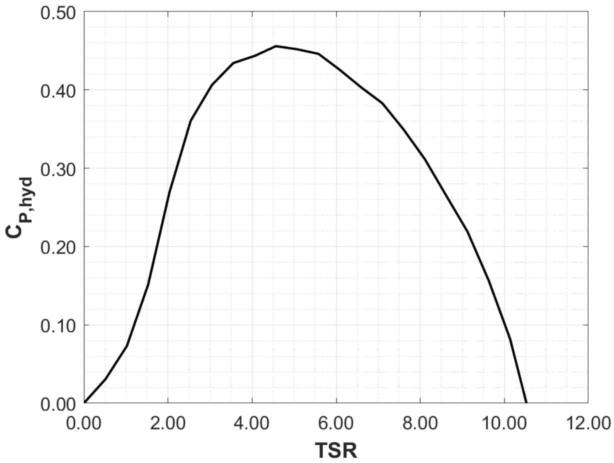

Fig. 12. Expected hydraulic power coefficient $c_{P,hyd}$ for one rotor of the GEMSTAR kite converter

To determine the mechanical efficiency coefficients, torque curves and hydraulic power curves obtained using the Blade Elements Momentum Theory (BEMT) were taken into account. The mechanical torque available to the generator shaft is the difference between the hydraulic torque available at the rotor and the hydraulic torque dissipated along the gearbox $T_{HYD}(n,V) - T_D(n)$. Indeed, it was necessary to take into account the main mechanical loss factors associated with the moving parts. Dissipated torque can be evaluated as follows:

$$T_D(n) = T_{D,gearbox}(n) + T_{D,bearings}(n) + T_{D,bellow\,seals}(n), \tag{9}$$

this is the sum of the torque derived from the gearbox, the rolling bearings and the axial seals of the bellows. The efficiency of the speed multiplier was assumed to be the value of 0.97 specified by the manufacturer.
With regard to the right-hand term of the Eq. 9, the torque $T_{D,gearbox}$ dissipated by the gearbox was assumed to be 97%, taking into account the nominal efficiency specified by the manufacturer. As for the power dissipated by the rolling bearings, the absorbed torque was calculated as specified in [32]. In particular, the following model was used to calculate the frictional torque of the bearings

$$T_{D,bearings}(n) = T_{rf}(n) + T_{sf}(n) + T_{bs}(n), \tag{10}$$

where M_{rf} is the rolling friction torque, M_{sf} is the sliding frictional moment and M_{bs} is the frictional moment of the two bearings seals. The third addend of the right-hand member of the Eq. [9] is the torque dissipated by bellow seals, which is calculated as follows:

$$T_{D,bellow\,seals}(n) = \eta_k \frac{D_m}{4} F_{preload} + K(n), \tag{11}$$

where η_k is the friction coefficient adopted for the sliding surfaces of the bellows seals acting on the average diameter D_m and $F_{preload}$ is the nominal preload force for the seal locking. The dynamic

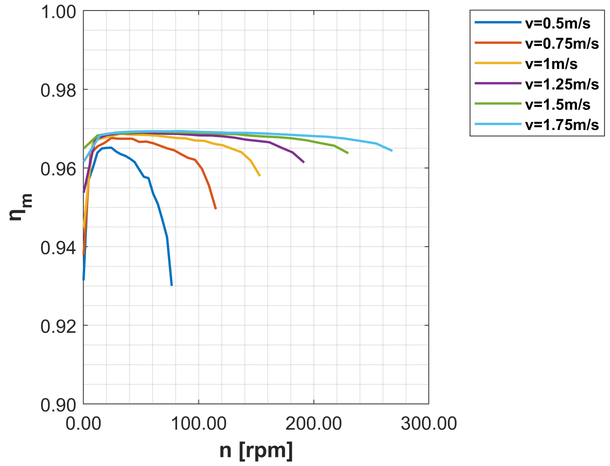

Fig. 13. Expected mechanical efficiency η_m of the GEMSTAR power transmission.

contribution $K(\omega)$ depends on the rotational speed and was considered negligible due to the low relative speed of the bellows friction surfaces. The friction coefficient has been considered both under static (equal to 0.51) and dynamic (equal to 0.23) conditions in a stationary regime. The value of the static friction coefficient was used to determine the starting torque of the turbine without electrical load. The ratio between mechanical power and hydraulic power was used to estimate the mechanical efficiency under steady-state conditions, at different rotational speeds and different current velocities. Further experimental investigations are carried out to verify this estimate. Figure 13 shows the values for the mechanical efficiency. Finally, the value of the required starting torque of 1.53 Nm was determined by adding the nominal starting torque of the electric generator without electric load. From the hydrodynamic interpolation shown in Figure 11 and by the relation 4, the value of the cut-in speed of 0.29 m/s was estimated.

VI. Data collection and system control

The monitoring and control system of the GEMSTAR tidal energy converter is essential for ensuring safe and efficient long-term operation in the marine environment. The architecture of the system has been designed to provide real-time data acquisition, fault detection and predictive maintenance capabilities, supporting both local control and remote monitoring. These features enable active attitude control, load management and power optimization depending on tidal stream conditions. The GEMSTAR system is equipped with an integrated network of sensors that monitors various operating parameters during deployment. These sensors are critical to ensuring system control and optimal energy generation. The most important parameters include:

- rotational speed, measured with encoders to track the performance of the rotor.
- Thrust force acting on the rotor blades, important for understanding hydrodynamic forces.
- Current speed and direction, monitored with an Acoustic Doppler Current Profiler (ADCP), which provides high-resolution current velocity profiles.
- Environmental conditions such as temperature and pressure that affect turbine performance
- Vibration level, which is monitored to detect early signs of mechanical wear in the drivetrain.

The sensors data are processed by an embedded Raspberry Pi-based unit (whose schematic is shown in Figure 14), which encapsulates the data into MQTT packets for reliable transmission over a TCP/IP network to the onshore control station. The control logic focuses on two main functions: optimization of power generation and attitude control. The system implements Maximum Power Point Tracking (MPPT) to adjust the rotation speed of the rotor to the speed of the current. The MPPT algorithm ensures that maximum power output is achieved in changing tidal conditions by dynamically adjusting the load [32]. The GEMSTAR device is capable of self-aligning with the direction of the tidal current. However, there are additional position control mechanisms to prevent cables from twisting and to ensure that the device is correctly aligned. This is achieved by feedback loops that adjust the rotational behaviour in response to changes in flow direction [33], [34]. The Fault Detection and Isolation (FDI) module continuously compares the real-time sensor data with the predictions of the digital twin. The FDI system identifies anomalies in performance and distinguishes between minor deviations, which can be corrected automatically, and critical failures, which require manual intervention.

All data is logged and stored for subsequent analysis. This allows researchers to: evaluate the efficiency of the system over time; identify long-term trends in energy production; detect early signs of mechanical problems that could affect performance. A number of criteria were taken into account when developing the hardware and software for data collection, namely

- soft real-time monitoring;
- control capabilities;
- logging of data in a flexible format;
- low-cost architecture for floodable parts;
- ease of reconfiguration.

More specifically, power generation management and optimization require direct knowledge of power generation on board and turbine speeds, which means that both the current and tension produced by the generators and the signals from the encoders installed in the generators must be measured. Load management follows the logic of maximum power point tracking to maximise the efficiency of energy conversion. Attitude control has two main objectives: to prevent the cables from twisting and to improve the alignment of the GEMSTAR with the current, thereby maximising power generation. For this reason, both the relative direction and the relative speed of sea current are measured by sensors installed on the device, while the undisturbed current direction and speed are measured by an ADCP installed near the device, in the undisturbed field. In addition, system attitude (with

TABLE III
SAMPLING FREQUENCIES OF DIFFERENT MEASUREMENTS.

Measurement	**Frequency (Hz)**
IMU measurements	1
Power (voltage and current)	50
Current angles	1
Generators speed	2
Flooding sensors	0.1

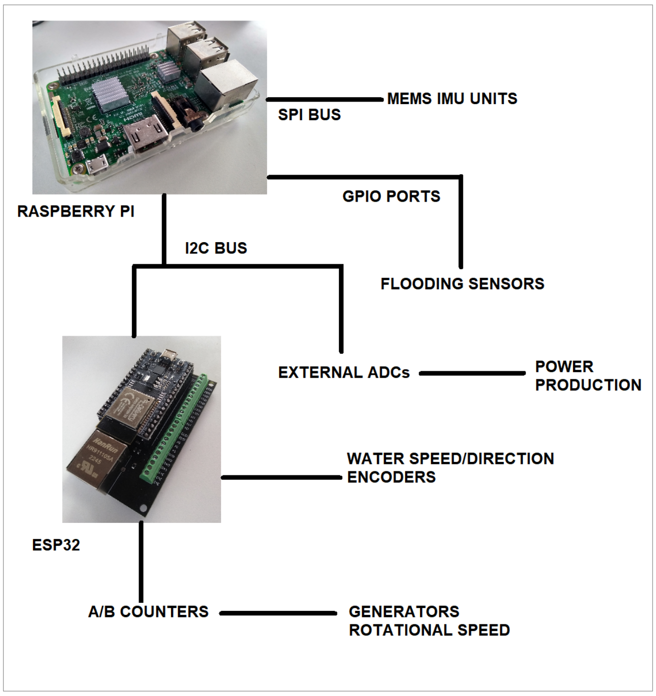

Fig. 14. A schema of the embedded data units on board.

MEMS [33] gyroscopes, accelerometers and compass sensors) and the cable tension (with a load cell) are measured. In addition, a pressure sensor on board will indicate the device quote. Actuation will rely on generators, on the one hand by selectively slowing down one of the turbines through load management, and on the other hand by switching the operating mode of the generators to that of the engine. For system monitoring, all of the above measurements are used together with the flood sensors in the lower tank of the GEMSTAR. The same data will also provide the inputs for a digital twin [34] of the GEMSTAR with fault detection and isolation capabilities. All three purposes of data acquisition can benefit from knowledge of the dynamic model of the system. However, some of its parameters, *e.g.* the inertia matrix, are difficult to determine with the required accuracy. Therefore, some parameters required for system monitoring and attitude control must be determined using an ad hoc system identification procedure that uses the collection of experimental data. The behaviour predicted by the model is compared with the measured behaviour of the device to validate the model.

Table III summarizes the sampling frequencies of the most relevant measurements.

VII. CONCLUSIONS

This work illustrates the design concepts and preliminary work for the long-term deployment of an underwater kite to generate electricity from tidal currents in the stretch of sea facing the RENEW-MEL laboratory, in the Strait of Messina. The characterization of the site is still ongoing, but it has already made it possible to define the preliminary design of the geometry of the kite and the turbines. Each element of the energy conversion chain has been characterized, or a suitable characterization method has been identified. The experiment will primarily allow the position control of the device, with a close connection to the optimization of energy production, also through an appropriate electrical load management. A digital twin of the device will also be developed, capable of detecting and isolating faults. Long-term deployment will allow the study of the effects of biofouling on system efficiency, for which a suitable method has been developed. Long-term deployment goes beyond previous work and is expected to be a necessary step towards the commercial exploitation of tidal energy. At the same time, it is expected that the necessary interdisciplinary efforts will lead to results that are of interest to several areas of research.

REFERENCES

[1] P. Bojek, "Renewable electricity," IEA: International Energy Agency, 2022.
[2] B. Guo, T. Wang, S. Jin, S. Duan, K. Yang, and Y. Zhao, "A review of point absorber wave energy converters," *Journal of Marine Science and Engineering*, vol. 10, no. 10, p. 1534, 2022.
[3] G. He, Z. Luan, W. Zhang, R. He, C. Liu, K. Yang, C. Yang, P. Jing, and Z. Zhang, "Review on research approaches for multi-point absorber wave energy converters," *Renewable Energy*, p. 119237, 2023.
[4] N. Delmonte, D. Barater, F. Giuliani, P. Cova, and G. Buticchi, "Review of oscillating water column converters," *IEEE Transactions on Industry Applications*, vol. 52, no. 2, pp. 1698–1710, 2015.
[5] L. Gurnari, P. G. Filianoti, and S. M. Camporeale, "Fluid dynamics inside a u-shaped oscillating water column (owc): 1d vs. 2d cfd model," *Renewable Energy*, vol. 193, pp. 687–705, 2022.
[6] G. Bevilacqua and B. Zanuttigh, "Overtopping wave energy converters: general aspects and stage of development," 2011.
[7] P. Contestabile, G. Crispino, E. Di Lauro, V. Ferrante, C. Gisonni, and D. Vicinanza, "Overtopping breakwater for wave energy conversion: Review of state of art, recent advancements and what lies ahead," *Renewable Energy*, vol. 147, pp. 705–718, 2020.
[8] L. Gurnari, P. G. Filianoti, M. Torresi, and S. M. Camporeale, "The wave-to-wire energy conversion process for a fixed u-owc device," *Energies*, vol. 13, no. 1, p. 283, 2020.
[9] N. Portillo Juan, V. Negro Valdecantos, M. D. Esteban, and J. S. López Gutiérrez, "Review of the influence of oceanographic and geometric parameters on oscillating water columns," *Journal of Marine Science and Engineering*, vol. 10, no. 2, p. 226, 2022.
[10] H. A. Said and J. V. Ringwood, "Grid integration aspects of wave energy—overview and perspectives," *IET Renewable Power Generation*, vol. 15, no. 14, pp. 3045–3064, 2021.
[11] D. P. Coiro, G. Troise, N. Bizzarrini, and G. Lazzerini, "Gemstar: A tethered system for tapping tidal currents energy," in *The 29th International Ocean and Polar Engineering Conference*. OnePetro, 2019.
[12] L. Blunden and A. Bahaj, "Tidal energy resource assessment for tidal stream generators," *Proceedings of The Institution of Mechanical Engineers Part A-journal of Power and Energy - PROC INST MECH ENG A-J POWER*, vol. 221, 03 2007.
[13] Black & Veatch ltd, "Carbon Trust Foreword to UK Tidal Current Resource and Economics Study," Carbon trust, Tech. Rep., 6 2011.

[14] S. B. Elghali, M. Benbouzid, and J. F. Charpentier, "Marine tidal current electric power generation technology: State of the art and current status," in *2007 IEEE International Electric Machines & Drives Conference*, vol. 2. IEEE, 2007, pp. 1407–1412.

[15] S. Walker and R. Howell, "Life cycle comparison of a wave and tidal energy device," *Proceedings of the Institution of Mechanical Engineers, Part M: Journal of Engineering for the Maritime Environment*, vol. 225, no. 4, pp. 325–337, 2011. [Online]. Available: https://doi.org/10.1177/1475090211418892

[16] C. Johnstone, D. Pratt, J. Clarke, and A. Grant, "A techno-economic analysis of tidal energy technology," *Renewable Energy*, vol. 49, pp. 101–106, 2013, selected papers from World Renewable Energy Congress - XI. [Online]. Available: https://www.sciencedirect.com/science/article/pii/S0960148112000651

[17] B. Guo, D. Wang, J. Zhou, W. Shi, and X. Zhou, "Performance evaluation of a submerged tidal energy device with a single mooring line," *Ocean Engineering*, vol. 196, p. 106791, 2020. [Online]. Available: https://www.sciencedirect.com/science/article/pii/S0029801819308911

[18] L. Perez, R. Cossu, A. Grinham, and I. Penesis, "An investigation of tidal turbine performance and loads under various turbulence conditions using blade element momentum theory and high-frequency field data acquired in two prospective tidal energy sites in australia," *Renewable Energy*, vol. 201, pp. 928–937, 2022. [Online]. Available: https://www.sciencedirect.com/science/article/pii/S0960148122016524

[19] D. Khojasteh *et al.*, "A large-scale review of wave and tidal energy research over the last 20 years," *Ocean Engineering*, vol. 282, p. 114995, 2023. [Online]. Available: https://www.sciencedirect.com/science/article/pii/S0029801823013793

[20] D. Coiro, G. Troise, F. Scherillo, A. De Marco, G. Calise, and N. Bizzarrini, "Development, deployment and experimental test on the novel tethered system gem for tidal current energy exploitation," *Renewable Energy*, vol. 114, pp. 323–336, 2017, wave and Tidal Resource Characterization. [Online]. Available: https://www.sciencedirect.com/science/article/pii/S0960148117300502

[21] D. P. Coiro, G. Troise, and N. Bizzarrini, "Experiences in developing tidal current and wave energy devices for mediterranean sea," *Frontiers in Energy Research*, vol. 6, 2018. [Online]. Available: https://www.frontiersin.org/articles/10.3389/fenrg.2018.00136

[22] D. Coiro, G. Troise, T. Ciuffardi, and G. Sannino, "Tidal current energy resource assessment: the strait of messina test case," in *2013 International Conference on Clean Electrical Power (ICCEP)*. IEEE, 2013, pp. 213–220.

[23] R. Morello, C. De Capua, P. Filianoti, and M. Lugarà, "A research laboratory for coastal and sea water pollution monitoring," in *6th EnvImeko-Imeko TC19–Second Edition Workshop on Environmental Instrumentation and Measurements, October 28, 2016, Reggio Calabria, Italy*, 2016, pp. 40–43.

[24] P. G. Filianoti and L. Gurnari, "A field experiment on wave forces on an energy-absorbing breakwater," *Energies*, vol. 13, no. 7, p. 1563, 2020.

[25] M. Massi, E. Salusti, and C. Stocchino, "On the currents in the strait of messina." *Il Nuovo Cimento*, vol. C 2, p. 543–548, 09 1979.

[26] R. Pawlowicz, B. Beardsley, and S. Lentz, "Classical tidal harmonic analysis including error estimates in matlab using t-tide," *Computers Geosciences*, vol. 28, no. 8, pp. 929–937, 2002. [Online]. Available: https://www.sciencedirect.com/science/article/pii/S0098300402000134

[27] D. Codiga, "Unified tidal analysis and prediction using the utide matlab functions," 09 2011.

[28] N. Milivojevic, M. Krishnamurthy, A. Emadi, and I. Stamenkovic, "Theory and implementation of a simple digital control strategy for brushless dc generators," *IEEE Transactions on Power Electronics*, vol. 26, no. 11, pp. 3345–3356, 2011.

[29] D. P. Coiro, G. Troise, T. Ciuffardi, and G. Sannino, "Tidal current energy resource assessment: The strait of messina test case," in *2013 International Conference on Clean Electrical Power (ICCEP)*, 2013, pp. 213–220.

[30] Z. Zhang, Y. Yan, S. Yang, and Z. Bo, "Development of a new permanent-magnet bldc generator using 12-phase half-wave rectifier," *IEEE Transactions on Industrial Electronics*, vol. 56, no. 6, pp. 2023–2029, 2009.

[31] Z. Zhou, M. Benbouzid, J.-F. Charpentier, F. Scuiller, and T. Tang, "Developments in large marine current turbine technologies – a review," *Renewable and Sustainable Energy Reviews*, vol. 71, pp. 852–858, 2017. [Online]. Available: https://www.sciencedirect.com/science/article/pii/S1364032116311698

[32] SKF Group, "The skf model for calculating the frictional moment." [Online]. Available: https://cdn.skfmediahub.skf.com/api/public/0901d1968065e9e7/pdf_preview_medium/0901d1968065e9e7_pdf_preview_medium.pdf

[33] E. D'Amato, V. A. Nardi, I. Notaro, and V. Scordamaglia, "A particle filtering approach for fault detection and isolation of uav imu sensors: Design, implementation and sensitivity analysis," *Sensors*, vol. 21, no. 9, 2021. [Online]. Available: https://www.mdpi.com/1424-8220/21/9/3066

[34] F. Ruffa, M. Lugarà, G. Fulco, D. Alizzio, F. Lo Savio, and C. De Capua, "Prognostic health management using ir thermography: The case of a digital twin of a niti endodontic file," *Sensors*, vol. 23, no. 9, 2023. [Online]. Available: https://www.scopus.com/inward/record.uri?eid=2-s2.0-85159153535&doi=10.3390%2fs23094296&partnerID=40&md5=4a1d9fe519e099a4c646bad3cc62d52a